PCCP

Accepted Manuscript

ROYAL SOCIETY OF CHEMISTRY

www.rsc.org/pccp

Molecular Modeling of Membrane Tube Pearling and the Effect of Nanoparticle Adsorption

Tongtao Yue [a], Xianren Zhang [b] and Fang Huang *[a]

[a]*State Key Laboratory of Heavy Oil Processing, Center for Bioengineering and Biotechnology, China University of Petroleum (East China), Qingdao, 266580, China. E-mail: fhuang@upc.edu.cn*

[b]*Division of Molecular and Materials Simulation, State Key Laboratory of Organic–Inorganic Composites, Beijing University of Chemical Technology, Beijing 100029, China.*

The shape transformation of membrane tubes, also known as pearling, is thought to play important roles in a variety of cellular activities, like intracellular transport. Despite considerable experiments investigating this phenomenon, the detailed molecular mechanism as well as how environmental factors affect the tube pearling instability is still ambiguous. In this work, we use computer simulation techniques to obtain molecular-level insight into the tube pearling process. We find that the tube morphology is strongly determined by the water pressure inside membrane tubes. For example, the tube shrinkage and subsequent bending is observed when we decrease the inner water pressure. Contrarily, as we increase the inner water pressure, the tube pearling tends to occur in order to reduce the surface energy. Besides, our simulations show that the membrane tube pearling is regulated by the adsorption of nanoparticles (NPs) in two competing ways. One is that the NP adsorption can exert additional membrane tension and thus promote the pearling and subsequent division of membrane tubes. On the other hand, the NP adsorption can locally rigidify the membrane and thus contrarily restrain the tube pearling. Therefore, NP size, NP concentration and NP-membrane adhesion strength will collectively regulate the tube pearling process.

1 Introduction

Lipid membrane tubes, which are ubiquitous in eukaryotic cells, play an essential role in a variety of cellular activities, like cell trafficking and intercellular communication.[1,2] Thus, understanding the molecular mechanism of membrane tubulation and subsequent shape transformation is of great importance for potential applications in biomaterials science and nanomedicine. Generally, the tubulation mechanism is extremely diverse. Besides the intrinsic factors, like spontaneous curvature, membrane asymmetry and membrane surface tension, it often requires accessory factors, such as clathrin or caveolin protein coats,[3] or motor proteins and external force.[4,5] The self assembly of BAR domain proteins on membrane surface is proved to induce and stabilize the membrane tubulation.[6-8] The physical mechanism driving the membrane tubulation by coating of membrane proteins is called the scaffolding mechanism. Our previous simulations showed that the membrane deformation even budding can be enhanced by the aggregation of anchored membrane proteins.[9] Besides, Šarić and Cacciuto showed that membrane tubes can be generated by linear aggregation of adhesion nanocomponents.[10] The linear aggregation of NPs on membrane surface was also observed in our previous simulation work.[11,12]

The shape transformation of membrane tubes, also known as pearling, is in some cases the onset in their cellular actions. In recent years, the mechanism of membrane tube pearling has been widely investigated both experimentally and theoretically. By perturbing the fluid membrane tubes with optical tweezers, Bar-Ziv and Moses first

discovered that the membrane tube pearling can be induced by competition of membrane curvature and membrane tension.[13, 14] This experimental observation was subsequently explained theoretically by Nelson *et al.*[15] Sparked by the work of Bar-Ziv and Moses, several successful investigations attempting to induce tension and thereby tube pearling have been performed.[16-18] For example, the membrane tension can also be generated by other factors, like polymer anchoring,[16,17,19] spontaneous curvature,[20,21] osmotic perturbation,[22,23] and external magnetic or electric field.[24,25] By anchoring polymers into oblate vesicles, a striking morphology change, including budding and tubulation, was observed by Tsafrir *et al.*[19] Previously, the same research group has reported the pearling instabilities of membrane tubes, also induced by anchoring of amphiphilic polymers.[16] Subsequently, the physical mechanism of pearling instabilities induced by polymers was confirmed by Campelo *et al.* using a phase-field model.[17] By using the Helfrich curvature elasticity theory, Wang *et al.* predicted the shapes of polymer anchored fluid vesicles.[26] Theoretically, Deuling and Helfrich predicted that membrane tubes with bilayers that have a non-zero spontaneous curvature can exhibit pearling.[20] Subsequently, a series of experimental findings were reported on pearling caused by spontaneous curvature that was induced by incorporation of another molecules, such as alkane or hydrophilic polymers with hydrophobic side groups along the backbone.[16,17,21]

Besides previous studies in which polymers and proteins formed membrane inclusions, the environmental stimulus is also reflected by the adsorption of NPs on membrane tube surface. By incorporating cationic NPs onto the inner leaflet of giant

unilamellar vesicles, Yu and Granick showed that the adsorption of NPs can increase the headgroup area of lipid molecules, and thus cause a mismatch of surface area between the outer and inner leaflets of the bilayer. The mismatch results in a spontaneous curvature and leads to wrinkling and consequent tube pearling.[27] However, when a number of negatively charged NPs is adsorbed onto the outer leaflet of liposomes, the stability and structure of liposomes can be controlled by tuning NP concentration.[28] Recently, Arai *et al.* systematically investigated the interaction of a janus or homogeneous NP with a vesicle.[29] By adjusting the initial velocity and chemical pattern of the NP, they found a variety of translocation dynamics and late-stage morphology of the vesicle-NP system. In our previous work, we have shown that the adsorption of ligand-coated NPs can rigidify the local lipid membrane and thus restrain the membrane bending.[11] Therefore, it will be more complicated when multiple NPs are adsorbed on the membrane tube surface. In the present work, we concentrate on the mechanism of membrane tube pearling and the effect of NP adsorption by using Dissipative Particle Dynamics (DPD) simulation techniques.

2 Models and Simulation Methods

2.1 Models

Within our simulations, each molecule is constructed by a number of beads. For example, the lipid model is constructed by connecting one hydrophilic head (H) and three hydrophobic beads (T). The H_1T_3 lipid model has been successfully used to study the dynamic properties of vesicles.[30] Here, in order to simulate the membrane

tube pearling process, 20000 lipid molecules were first arranged along a cylindrical surface with diameter of 30 nm and length of 100 nm. In order to eliminate the effects of predefined initial configuration and balance the pressure difference between the inside and outside of the membrane tube, the system was relaxed at the higher temperature of 2.0 for 50000 time steps, and then annealed slowly to T=1.0. After 100000 time steps equilibrium simulation, a number of ligand-coated NPs are placed onto the outer leaflet of membrane tubes. Each NP is constructed by arranging a number of hydrophilic beads (P) and is constrained to move as a rigid body. In order to study the effect of NP-membrane adhesion strength on the membrane tube pearling, a number of ligand beads (L) is coated on the NP surface, and they are set to interact with the hydrophilic bead of each lipid. Solvent molecules (W), which are modeled as single beads, and other components are not allowed to enter the interior of NPs. We also adjusted the number of water beads inside membrane tubes to modulate the membrane tension and thus regulate the shape transformation. All simulations were performed in an NVT ensemble with a box size of 75nm×75nm×100nm.

2.2 Simulation methods

The simulations presented in this work are based on the Dissipative Particle Dynamics (DPD) method, which is a coarse-grained simulation technique with hydrodynamic interactions. The DPD simulation method was first introduced to simulate the hydrodynamic behavior of complex fluids.[31-33] Recently, it was proved to be especially useful to investigate the mesoscale behaviors of lipid membranes.[34-41] In

DPD methods, the elementary units are soft beads whose dynamics are governed by Newton's equation of motion, $\frac{dr_i}{dt} = v_i$ and $\frac{dv_i}{dt} = \frac{f_i}{m}$, similar to Molecular Dynamics method. Beads *i* and *j* interact with each other via a pairwise additive force consisting of a conservative force F_{ij}^C, a dissipative force F_{ij}^D and a random force F_{ij}^R. So the total force exerted on bead *i* is expressed as

$$F_i = \sum_{i \neq j} (F_{ij}^C + F_{ij}^D + F_{ij}^R) \tag{1}$$

The conservative force between beads *i* and *j* is soft repulsion acting along the line of the particle centers and is determined by

$$F_{ij}^C = a_{ij} \tilde{r}_{ij} \max\{1 - r_{ij}/r_c, 0\} \tag{2}$$

where a_{ij} is the maximum repulsive strength between beads *i* and *j*, $\boldsymbol{r_{ij}} = \boldsymbol{r_j} - \boldsymbol{r_i}$ ($\boldsymbol{r_i}$ and $\boldsymbol{r_j}$ are their positions), $r_{ij} = |\boldsymbol{r_{ij}}|$, $\tilde{r}_{ij} = \boldsymbol{r_{ij}}/|r_{ij}|$, and r_c is the cutoff radius.

The dissipative force has the form,

$$F_{ij}^D = -\gamma (1 - r_{ij}/r_c)^2 (\tilde{r}_{ij} \cdot v_{ij}) \tilde{r}_{ij} \tag{3}$$

where γ is the friction coefficient, $v_{ij} = v_i - v_j$ (v_i and v_j are their velocities). The expression is chosen to conserve the momentum of each pair of particles and thus the total momentum of the system is conserved.

The random force also acts between each pair of particles as

$$F_{ij}^R = -\sigma (1 - r_{ij}/r_c)^2 \theta_{ij} \tilde{r}_{ij} \tag{4}$$

where σ represents the noise amplitude, and θ_{ij} is an uncorrelated random variable with zero mean and unit variance.

For lipid molecules, the interaction between neighboring beads in the same molecule is described by a harmonic spring force:

$$F_S = K_S(r_{ij} - r_{eq})\tilde{r}_{ij} \tag{5}$$

where K_S is the spring constant and r_{eq} is the equilibrium bond length. The numerical value of K_S and r_{eq} used for our simulation are 128.0 and 0.7, respectively. The force constraining the variation of the bond angle is given by

$$F_\varphi = -\nabla U_\varphi \quad \text{and} \quad U_\varphi = K_\varphi(1-\cos(\varphi - \varphi_0)) \tag{6}$$

where φ_0 is set to π and K_φ, the bond bending force constant, is set to 10.0. The time evolutions of the systems were obtained from a modified version of Velocity-Verlet algorithm with a time step of Δt =0.02.

In the pure membrane system, the interaction parameters a_{ij} between the same bead types were set to $a_{hh} = a_{tt} = a_{ww}$ =25, and those between different bead types were a_{ht} = 200, a_{hw} =25, a_{tw} =200. Besides, in order to study the effect of NP-membrane adhesion strength on membrane tube pearling, the ligand-lipid interaction parameter a_{LH} is varied from 0.0 and 10.0, which represent strong and weak NP-membrane interaction, respectively.

3 Simulation results and discussion

In our simulations, we change the number of water beads inside membrane tubes (N_{in}) to adjust the membrane pressure and further regulate the morphology transformation. For example, we find that the cylindrical morphology of membrane tubes is well maintained as we fix the value of N_{in} to about 48000. In fact, we count the number of water beads inside the membrane tube to 47121 after the annealing simulation. Therefore, the value of N_{in}=48000 can approximately represent the zero

pressure difference between inside and outside of the tube. Accordingly, as we add or delete a number of water beads from inside of the membrane tube, the membrane pressure is correspondingly changed. As a result, two different shape transformation pathways are observed. They are membrane tube shrinking and subsequent bending and tube pearling, respectively. Both dynamics and molecular mechanism of the two pathways will be discussed in the following two sections. In section 3.3 and 3.4, the promotive and restraining effect of NP adsorption on membrane tube pearling will be analyzed, and the resultant effect of NP size and concentration is summarized in a phase diagram given in section 3.5.

3.1 Shrinking and subsequent bending of membrane tubes

When N_{in}=28000, the water pressure inside the membrane tube is strikingly decreased. In order to rebalance the pressure across the membrane, the membrane tube first undergoes a striking shrinkage. Correspondingly, the tube shrinkage is accompanied by the decrease of membrane tension due to the decrease of lipid area. As a result, the subsequent morphology transformation is strongly affected in two separate directions. In the horizontal direction, the spherical cross section of the tube gradually turns to be elliptical (Fig. 1, t=60000). In the vertical direction, the membrane tube then starts to bend along the shorter ellipsoidal radius (Fig. 1, t=100000), and finally an S-shaped membrane tube is formed (Fig. 1, t=200000). The specific membrane tube bending direction is based on the theory that the bending rigidity of one cylindrical nanotube is strongly dependent on its aspect ratio.

Generally, the bending rigidity increases with the tube width when the tube length is fixed. In the specific case, the membrane tube bending rigidity is much smaller along the shorter radius than that of the longer radius. Namely, bending along the shorter radius is more energetically favorable than the longer radius. Besides, it is noted that the shape transformation pathway of membrane tubes is distinct from that of planar membranes. For two-dimensional planar lipid membranes, decreasing membrane tension can simply induce the membrane deformation, although the existence of membrane proteins may induce membrane budding and tubulation. For cylindrical membrane tubes, however, the situation is more complicated due to the nature of shape anisotropy. In general, the whole morphology transformation process is divided into three stages. In the first stage, the membrane tube undergoes a transient but striking shrinkage in order to rebalance the water pressure across the membrane. Meanwhile, the tube shrinkage is accompanied by the decrease of membrane tension, which further affects the subsequent morphology transformation. The second stage is characterized by the transition of tube cross section from spherical to elliptical shape. In the last stage, the tube starts to bend along the shorter ellipsoid radius and finally forms an S-shaped membrane tube.

3.2 Pearling of membrane tubes

When we fixed the number of water beads inside membrane tubes (N_{in}) to 66000, the membrane tube pearling occurs. Both typical snapshots and time evolution of total membrane area are shown in Fig. 2. After the addition of water beads into the

membrane tube, the inner water pressure is largely increased. As a result, the membrane tube first undergoes a transient swelling in order to rebalance the water pressure across the membrane. Meanwhile, the tube swelling is accompanied by the increase of membrane tension due to the increase of lipid area. We review that the increased membrane tension tends to shrink lipid membranes into smaller area. Therefore, the resultant increase of membrane tension can be released by the subsequent tube pearling (Fig. 2A). This is distinct from the case of vesicles, in which the increase of inner water pressure will homogeneously enlarge the vesicle size and the resultant tension could not be released by further transition. In the pearling process, the initial heterogeneous distribution of the tube radius is quite crucial because the membrane tube always shrink first at the location where the radius is slightly smaller than other regions (Fig. 2A). This is critical because the real membrane tubes are not strictly cylindrical, which means the heterogeneous distribution of membrane tube radius is ubiquitous in cell. As the simulation proceeds, the local radius of the shrinking point continues to decrease while the region with larger radius tends to swell (Fig. 2A, t=50000). At last, the whole membrane tube transits into two vesicles, which are connected by a cylindrical micelle (Fig. 2A, t=300000). The pearling phenomenon can be illustrated more clearly as we remove the periodic boundary condition and connect four pearled membrane tubes into a longer one (Fig. 2A, lower snapshot).

It has been experimentally and theoretically proved that the membrane tube pearling is induced by competition of membrane curvature and membrane

tension.[13-15,42,43] In most experiments, the pearling is generally caused by addition of foreign matters, like adsorbing NPs or anchoring amphiphilic molecules.[16,17,19,27] The electric or magnetic field is also proved to induce the tube pearling transition.[24,25] In the present work, we speculate that the tube pearling transition is mainly induced by the increased membrane surface energy. Specifically, the membrane surface energy is determined by the membrane tension and membrane area. However, due to the difficulty in calculating the membrane tension of cylindrical tubes, we are not able to quantitatively express the membrane surface energy. Nevertheless, we monitored the evolution of total membrane area during the simulation (Fig. 2B). This is informative because the decrease of membrane area under increase inner water pressure can only be ascribed to the increased membrane tension. In other words, the evolution of total membrane area can qualitatively reflect the release of high membrane surface energy.

According to Fig. 2B, the whole evolution can be divided into three stages. The first stage is characterized by a drastic oscillation. This is induced by the drastic increase of inner water pressure by adding water beads into the tube. After that, due to the increase of membrane tension, the tube area undergoes a sharp decrease, which corresponds to the membrane tube pearling process. In the last stage, the pearled membrane tube is relatively stable and no fission of the neck is observed during our simulation. In fact, the fission of the neck, also known as pearling division, is generally accelerated by an external force, which can be generated by actin polymerization or Sar1.[44-47] In the following section, we will show that in some cases the tube pearling and subsequent division can be promoted by adsorption of NPs,

although in some other cases the tube pearling can also be restrained by the NP adsorption.

3.3 Promotion of membrane tube pearling by NP adsorption.

It is noteworthy that no pearling or pearling division occurs if we fix the water number inside membrane tubes to 48000, even with NP adsorption (data not shown). Namely, the effect of NP adsorption on membrane tube pearling is secondary compared with the water pressure inside membrane tubes. Therefore, in the following, we fixed the number of water beads inside the membrane tube to 66000 to investigate the effect of NP adsorption.

First, we fixed the NP diameter to 2.5nm, which is smaller than the membrane thickness. According to the typical snapshots (Fig. 3A) and time evolution of average NP wrapping extent (Fig. 3B), NPs are partially wrapped by membrane due to the small NP size.[48,49] Compared with membrane tubes in the absence of NPs (Fig. 2), the effect of NPs with a number of 20 is negligible to the membrane tube pearling because the distribution of tube radius is quite stable after t=15000 and no tube fission is observed during our simulation (Fig. 3C). Nevertheless, we note that all NPs escape from the membrane neck and preferentially locate at the 'vesicle' surface (Fig. 3D). Besides, it is well understood that the NP adhesion can exert membrane tension[50,51] and thus may promote the tube pearling. Therefore, we speculate that if we increase the NP number or NP wrapping extent, the membrane tension will be further increased and correspondingly the tube pearling and subsequent division should be

strongly promoted. To this end, we first fix the NP diameter to 2.5nm and increase the NP number to 30. According to the typical snapshots, a similar pearling transition is observed in the early stage (Fig. 4A, t<200000). Subsequently, due to the increase of NP number, the membrane tension exerted by the NP adsorption is further increased (Fig. 4B). As a result, the radius of the membrane neck starts to decrease after the complete of tube pearling. At last, the pearling division and correspondingly a transition from membrane tube to vesicle is observed (Fig. 4C). Likewise, as we fixed the NP number to 20 and just increase the NP diameter from 2.5nm to 3.8nm, which is approximate to the membrane thickness, a similar tube pearling and subsequent division is observed (Fig. 5A). In this case, increasing the NP size can on one hand increase the average NP wrapping extent (Fig. 5B). On the other hand, the total wrapping area is increased for larger NPs. Therefore, the membrane tension exerted by NPs can be further increased by increasing the NP size. Nevertheless, we note that if we further increase the NP size or NP concentration, the membrane tube pearling will contrarily be restrained by the NP adsorption. The detailed restraining mechanism will be discussed in the following section.

The pearling and subsequent division of membrane tubes in the present of NP adsorption is clearly reflected by the time evolution of membrane tube area (Fig. 6). After the initial high frequent oscillation, which is induced by the addition of water beads into the membrane tube, the tube area undergoes two sharp decreases. The first decrease corresponds to the membrane tube pearling process (Fig. 5A), which is similar to the case without NP adsorption (Fig. 2B). Differentially, the pearled

membrane tube is unstable due to the further decreased membrane tension by NP adsorption. The fission of membrane neck and subsequent tube-vesicle transition thus occurs which is reflected by the second decrease of membrane tube area (Fig. 6).

In order to further understand the promotive effect of NP adsorption on membrane tube pearling, we fixed the NP diameter and NP number to 2.5nm and 30, respectively, and decrease the NP-membrane adhesion strength by increasing the corresponding interaction parameter a_{LH} from 0.0 to 10.0. As shown in the typical snapshots (Fig. 7A) and time evolution of average NP wrapping percentage, all NPs are just slightly wrapped by the membrane and move more freely on the membrane tube surface. Therefore, according to the distributions of membrane tube radius (Fig. 7C), the effect of NP adsorption on membrane tube pearling is negligible as we decrease the NP-membrane adhesion strength. Therefore, our simulation results further confirm that the promotive effect of NP adsorption on membrane tubes pearling is mainly ascribed to the extra membrane tension exerted by the NP wrapping, the extent of which is well tuned by regulating the NP size, NP concentration and NP-membrane adhesion strength.

3.4 Restraining of membrane tube pearling by NP adsorption

In our previous simulation work, we have mentioned that the adsorption of NPs can locally rigidify the membrane and thus restrain the membrane deformation.[11] Besides, the membrane tube pearling is a result of competition of membrane tension and membrane curvature.[13] Therefore in this work, we speculate that the adsorption of

NPs on the membrane tube surface may in some extent rigidify the membrane and thus restrain the membrane tube pearling. Moreover, we notice that during the membrane tube pearling process, the initial uniformly distributed NPs tend to escape from the membrane neck location and gradually move to the 'vesicle' area (Fig. 3-5). The preferential location of NPs is mainly ascribed to the heterogeneous distribution of membrane curvature. Specifically, it will spend more membrane bending energy to wrap a NP for a membrane with a larger positive curvature than with a smaller curvature. During the pearling process, the curvature of 'neck' surface is apparently larger than that of 'vesicle' surface. Therefore, the preferential location of NPs on the 'vesicle' surface is energetically favorable. Moreover, the distribution as well as arrangement of multiple NPs on the membrane surface is on one hand determined by the nature of membrane mediated interaction, which can be modulated by changing the NP size[11] and shape,[12] while the other important factor is the NP concentration.[11,52] In our previous work, we have shown that the endocytosis of multiple NPs is in fact a cooperative process, and the cooperative effect is dependent on NP size, membrane tension and NP concentration.[11] Correspondingly in the present work, we want to further increase the NP size and concentration to understand its effect on the membrane tube pearling process.

First, we placed 30 NPs with diameter of 7.5nm on the membrane tube surface. According to the typical snapshots (Fig. 8A) and time evolution of average NP wrapping percentage (Fig. 8B), the NP wrapping extent is apparently decreased although the NP size is largely increased. This is because the higher membrane

tension exerted by the NP adsorption conversely weakens their wrapping extent. Besides, we note that the extent of heterogeneity of final distribution of NPs along the membrane tube is largely weakened (Fig. 8C). Consequently, the bending rigidity of the membrane tube is strengthened by the NP adsorption and the membrane tube pearling is thus restrained. Similarly, as we fixed the NP diameter to 3.8nm and further increase the NP number to 80, the cylindrical shape of membrane tubes is strongly maintained and no membrane tube pearling occurs during our simulation (Fig. 9). Therefore, the membrane tube pearling can be effectively restrained by further increase of the NP size or NP concentration.

In order to energetically understand the restraining effect of NPs on the membrane tube pearling, we calculate the evolution of tube area during our simulation (Fig. 10). The NP diameter and number are fixed to 3.8nm and 80, respectively. We notice that after a drastic oscillation, no obvious decrease of the area is observed. This is distinct from the situation in Fig. 2 and Fig. 6, where a sharp decrease of tube area is observed. In general, the high membrane surface energy induced by the increase of membrane tension can be effectively reduced by membrane tube pearling. Meanwhile, the tube pearling process is accompanied by the increase of membrane bending energy, which is unfavorable to the pearling process. Therefore, the local membrane bending rigidity is quite important in the pearling process. In the present case, the membrane bending rigidity is strongly enhanced by NP adsorption. Therefore, the cylindrical shape of the membrane tube is maintained and no tube pearling is observed during the simulation.

3.5 Phase diagram

According to the above simulation results, we find that the membrane tube pearling is mainly induced by the increase of membrane tension, which is accomplished by increasing the water pressure inside the membrane tubes. When NPs are adsorbed onto the outer leaflet of membrane tubes, the membrane tension can be further increased. As a result, the membrane tube pearling is promoted by the NP adsorption. In some other cases, contrarily, the membrane tube pearling is restrained by the NP adsorption because of the increased membrane bending rigidity. Therefore, the resultant effect of NP adsorption on membrane tube pearling is a competition of the increased membrane tension exerted by NP adsorption and the increased membrane bending rigidity, also induced by the NP adsorption. Moreover, the increased membrane tension can reduce the NP wrapping extent, which may modulate the NP arrangement by changing the nature of membrane mediated NP interaction. The detailed effect of NP adsorption on membrane tube pearling is summarized in the phase diagram as a function of NP diameter and NP number (Fig. 11). The figure indicate that the effect of NP adsorption on membrane tube pearling can be negligible, promotive, and restraining, depending on the NP size and NP concentration.

In general, the effect of NP adsorption on membrane tube pearling is negligible when both NP size and NP concentration is small enough. This is because the membrane tension as well as membrane bending rigidity induced by NP adsorption is too weak to affect the membrane tube pearling. For smaller NPs, the membrane tube pearling as well as subsequent division can be promoted by increasing the NP

concentration. However, as we further increase the NP concentration, the increase of membrane tension will stop because of the decreased NP wrapping extent (Fig. 9B). Contrarily, the strengthening of membrane bending rigidity is always continuous as we further increase the NP concentration. Therefore, the membrane tube pearling turns to be restrained by further increase of NP concentration. Likewise, the transition from promotive effect to restraining effect can also be achieved by further increase of the NP size (Fig. 11).

4 Conclusions

Membrane tube pearling is in some cases the onset in their cellular actions. Therefore, understanding how membrane tube pearling occurs especially how environmental factors affect the pearling instability is of quite importance for potential applications in biomaterials science and nanomedicine. In this paper, using Dissipative Particle Dynamics simulations, we reproduced the membrane tube pearling process from model membranes. These simulations gave detailed structural information on membrane tube pearling, and provide a link between molecular simulation and membrane material properties.

Our simulations show that the membrane tube pearling is mainly induced by the increased membrane tension. Specifically, as we increase the water pressure inside the membrane tube, the membrane tube first undergoes a swelling in order to rebalance the pressure across the membrane. Meanwhile, the membrane tube swelling is accompanied by the increase of membrane tension, which is subsequently released by

the tube pearling.

By introducing NPs onto the outer leaflet of membrane tubes, our simulations indicate that the membrane tube pearling can be promoted or restrained by NP adsorption. The promotive effect is because of the extra membrane tension exerted by the NP adsorption, while the restraining effect is ascribed to the NP-induced membrane bending rigidity. In more detail, the nature of effect is dependent on several factors, including the NP size, NP concentration and NP-membrane adhesion strength. The effect of NP size and concentration is described in the phase diagram presented here (Fig. 11). In the aspect of NP-membrane adhesion strength, increasing the NP-membrane adhesion strength can enhance the NP wrapping extent and thus exert larger membrane tension. On the other hand, different wrapping extent may have some critical effect on the nature of membrane mediated NP interaction and thus affect their distribution and arrangement on the membrane tube surface. This may further modulate the membrane tube pearling process.

Acknowledgements

This work was financially supported by National Natural Science foundation of China (No. 21303269, No. 21276007, No. 21073236, and No. 21033005), the program for New Century Excellent Talents in University of Ministry of Education of China (NCET-10-0815), and the Natural Science Foundation for Distinguished Young Scholar of Shandong Province (No. JQ201008). T. YUE Thanks the support of Natural Science foundation of Shandong Province (No. ZR2013BQ029), Qingdao

Science and Technology Project (No. 13-1-4-235-jch), and the Fundamental Research Funds for the Central Universities. The authors thank the National Supercomputing Center in Jinan for providing computer time.

References

1 B. Alberts, A. Johnson, J. Lewis, M. Raff, K. Roberts and P. Walter, *Molecular Biology of the cell*, New York, Garland Science, 5th edition, 2007.

2 P. Sens, L. Johannes and P. Bassereau, *Curr. Opin. Cell Biol.*, 2008, **20**, 476-482.

3 K. Farsad and P. De Camili, *Curr. Opin. Cell Biol*., 2003, **15**, 372-381.

4 G. Koster, A. Cacciuto, I. Derényi, D. Frenkel and M. Dogterom, *Phys. Rev. Lett.*, 2005, **94**, 068101.

5 S. Baoukina, S. J. Marrink and D. P. Tieleman, *Biophys. J*., 2012, **102**, 1866-1871.

6 J. Zimmerberg and M. M. Kozolv, *Nat. Rev. Mol. Cell Biol.*, 2006, **7**, 9-19.

7 H. Cui, C. Mim, F. X. Vázquez, E. Lyman, V. M. Unger and G. A. Voth, *Biophys. J*., 2013, **104**, 404-411.

8 C. Mim, H. Cui, J. A. Gawronski-Salerno, A. Frost, E. Lyman, G. A. Voth and V. M. Unger, *Cell*, 2012, **149**, 137-145.

9 T. Yue, S. Li, X. Zhang and W. Wang, *Soft Matter*, 2010, **6**, 6109-6118.

10 A. Šarić and A. Cacciuto, *Phys. Rev. Lett.*, 2012, **109**, 188101.

11 T. Yue and X. Zhang, *ACS Nano*, 2012, **6**, 3196-3205.

12 T. Yue, X. Wang, F. Huang and X. Zhang, *Nanoscale*, 2013, **5**, 9888-9896.

13 R. Bar-Ziv and E. Moses, *Phys. Rev. Lett.*, 1994, **73**, 1392-1395.

14 R. Bar-Ziv, T. Tlusty, E. Moses, S. A. Safran and A. Bershadsky, *Proc. Natl. Acad. Sci. USA*, 1999, **96**, 10140-10145.

15 P. Nelson and T. Powers, *Phys. Rev. Lett.*, 1995, **74**, 3384-3387.

16 I. Tsafrir, D. Sagi, T. Arzi, M. Guedeau-Boudeville and V. Frette, *Phys. Rev. Lett*., 2001, **86**, 1138-1141.

17 F. Campelo and A. Hernández-Machado, *Phys. Rev. Lett.*, 2007, **99**, 088101.

18 T. F. Zhu, K. Adamala, N. Zhang and J. W. Szostak, *Proc. Natl. Acad. Sci. USA*, 2012, **109**, 9828-9832.

19 I. Tsafrir, Y. Caspi, M. Guedeau-Boudeville, T. Arzi and J. Stavans, *Phys. Rev. Lett.*, 2003, **91**, 138102.

20 H. J. Deuling and W. Helfrich, *Biophys. J*., 1976, **16**, 861-868.

21 S. Chaïeb and S. Rica, *Phys. Rev. E*, 1998, **58**, 7733-7737.

22 M. Yanagisawa, M. Imai and T. Taniguchi, *Phys. Rev. Lett*., 2008, **100**, 148102.

23 M. Yanagisawa, N. Shimokawa, M. Ichikawa and K. Yoshikawa, *Soft Matter*, 2012, **8**, 488-495.

24 C. Mnager, M. Meyer, V. Cabuil, A. Cebers, J. –C. Bacri and R. Perzynski, *Eur. Phys. J. E*, 2002, **7**, 325-337.

25 K. P. Sinha, S. Gadkari and R. M. Thaokar, *Soft Matter*, 2013, **9**, 7274-7293.

26 J. Wang, K. Guo, F. Qiu, H. Zhang and Y. Yang, *Phys. Rev. E*, 2005, **71**, 041908.

27 Y. Yu and S. Granick, *J. Am. Chem. Soc*., 2009, **131**, 14158-14159.

28 R. Michel, T. Plostica, L. Abezgauz, D. Danino and M. Gradzielski, *Soft Matter*,

2013, **9**, 4167-4177.

29 N. Arai, K. Yasuoka and X. C. Zeng, *Nanoscale*, 2013, **5**, 9089-9100.

30 M. Laradji and P. B. Sunil Kumar, *Phys. Rev. Lett.*, 2004, **93**, 198105.

31 P. J. Hoogerbrugge and J. M. V. A. Koelman, *Europhys. Lett.*, 1992, **19**, 155-160.

32 P. Español and P. Warren, *Europhys. Lett.*, 1995, **30**, 191-196.

33 R. D. Groot and P. B. Warren, *J. Chem. Phys.*, 1997, **107**, 4423-4435.

34 J. C. Shillcock and R. Lipowsky, *Nat. Mater.*, 2005, **4**, 225-228.

35 A. Grafmüller, J. Shillcock and R. Lipowsky, *Phys. Rev. Lett.*, 2007, **98**, 218101.

36 L. Gao, R. Lipowsky and J. Shillcock, *Soft Matter*, 2008, **4**, 1208-1214.

37 K. Yang and Y. Ma, *Nat. Nanotechnol.*, 2010, **5**, 579-583.

38 K. Yang, B. Yuan and Y. Ma, *Nanoscale*, 2013, **5**, 7988-8006.

39 Y. Li, X. Li, Z. Li and H. Gao, *Nanoscale*, 2012, **4**, 3768-3775.

40 S. Li, X. Zhang, W. Dong and W. Wang, *Langmuir*, 2008, **24**, 9344-9353.

41 T. Yue and X. Zhang, *Phys. Rev. E: Stat., Nonlinear, Soft Matter Phys.*, 2012, **85**, 011917.

42 P. A. Pullarkat, P. Dommersnes, P. Fernández, J. Joanny and A. Ott, *Phys. Rev. Lett.*, 2006, **96**, 048104.

43 J. Sanborn, K. Oglecka and R. S. Kraut, *Faraday Discuss.*, 2013, **161**, 167-176.

44 R. L. Jeng and M. D. Welch, *Curr. Biol.*, 2001, **11**, R691-R694.

45 M. Kaksonen, C. P. Toret and D. G. Drubin, *Nat. Rev. Mol. Cell Biol.*, 2006, **7**, 404-414.

46 B. J. Galletta and J. A. Cooper, *Curr. Opin. Cell Biol.*, 2009, **21**, 20-27.

47 B. Antonny, *Curr. Opin. Cell Biol.*, 2006, **18**, 386-394.

48 H. Gao, W. Shi and L. B. Freund, *Proc. Natl. Acad. Sci. USA*, 2005, **102**, 9469-9474.

49 S. Zhang, J. Li, G. Lykotrafitis, G. Bao and S. Suresh, *Adv. Mater.*, 2009, **21**, 419-424.

50 S. Li and N. Malmstadt, *Soft Matter*, 2013, **9**, 4969-4976.

51 T. Yue and X. Zhang, *Soft Matter*, 2011, **7**, 9104-9112.

52 X. Chen, F. Tian, X. Zhang and W. Wang, *Soft Matter*, 2013, **9**, 7592-7600.

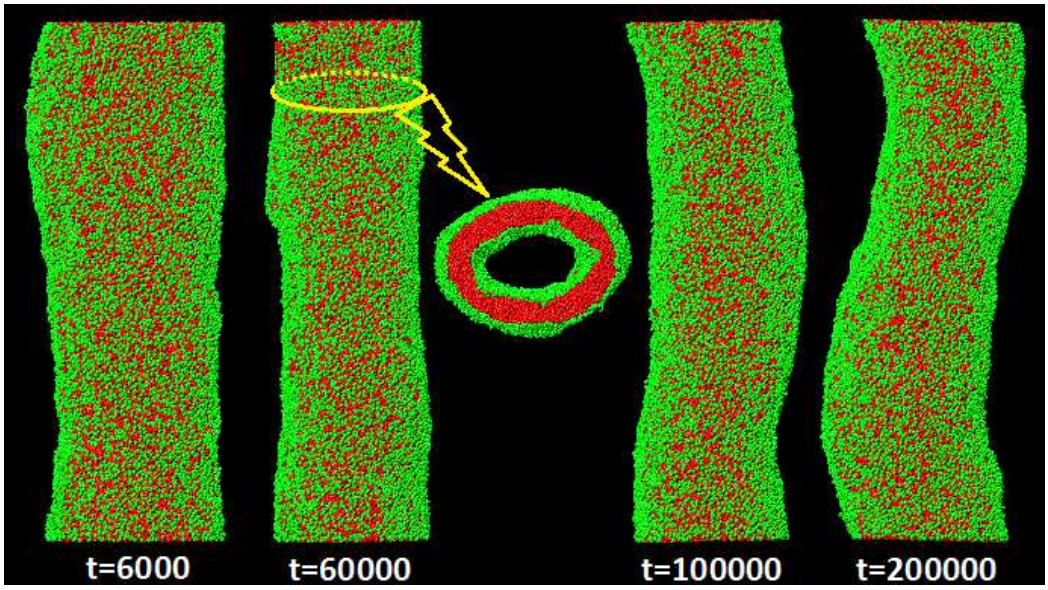

Fig. 1 Time sequence of snapshots corresponding to the shape transformation of membrane tube with 28000 water beads inside the tube. The middle snapshot shows the cross section of the membrane tube at t=60000.

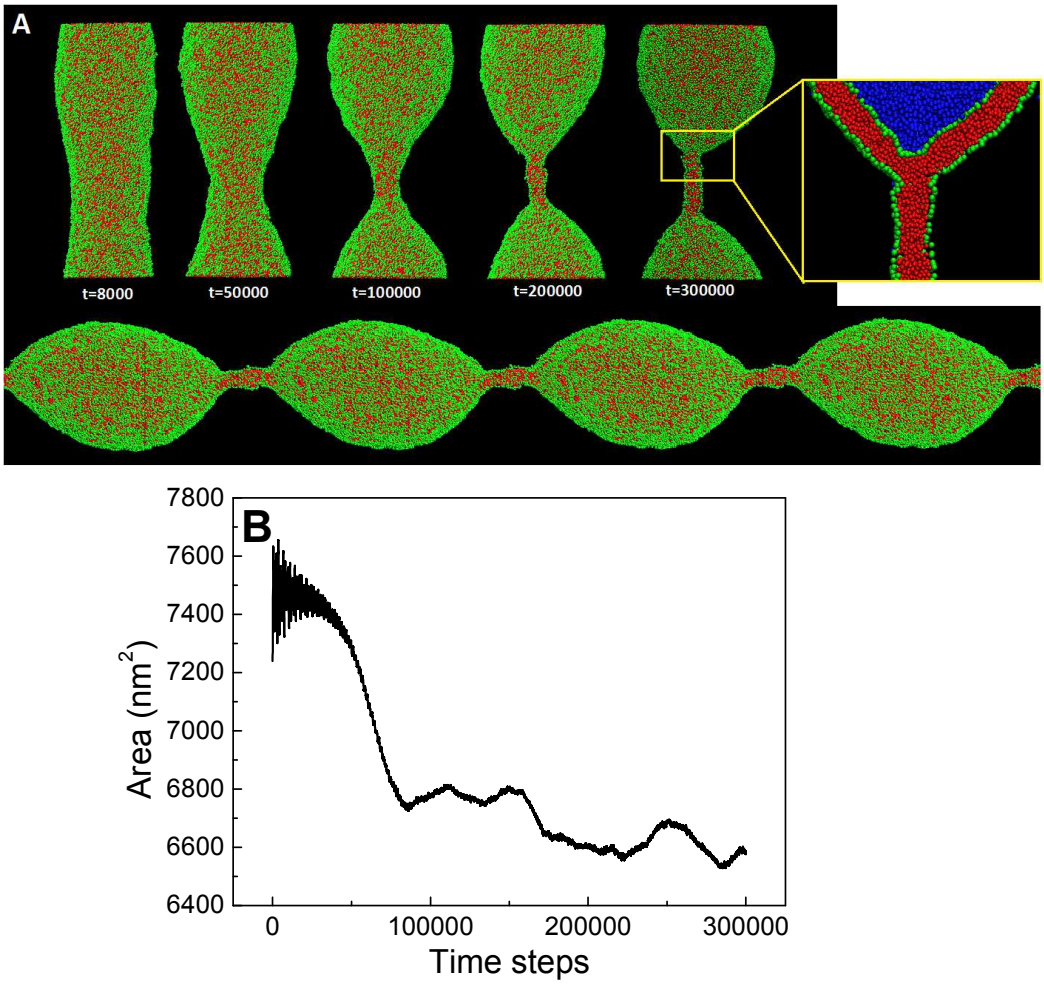

Fig. 2 (A) Time sequence of snapshots corresponding to the pearling of membrane tube with 66000 water beads inside the tube. The lower figure shows the long pearled tube which is connected by four shorter tubes. (B) Time evolution of membrane tube area during the pearling process.

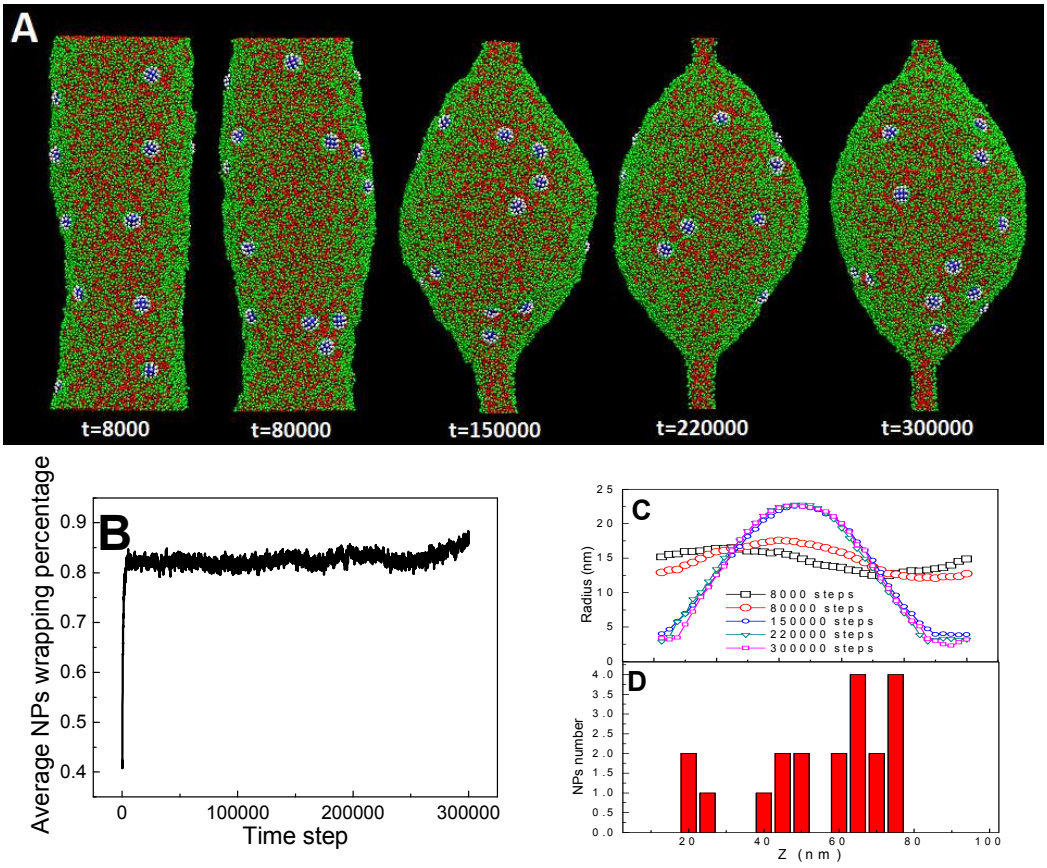

Fig. 3 The negligible effect of NPs with diameter and number of 2.5nm and 20 on the membrane tube pearling. A shows the time sequence of typical snapshots, B shows the time evolution of average wrapping extent of NPs, C shows the corresponding distribution of membrane tube radius, and D shows the final distribution of NPs along membrane tube direction.

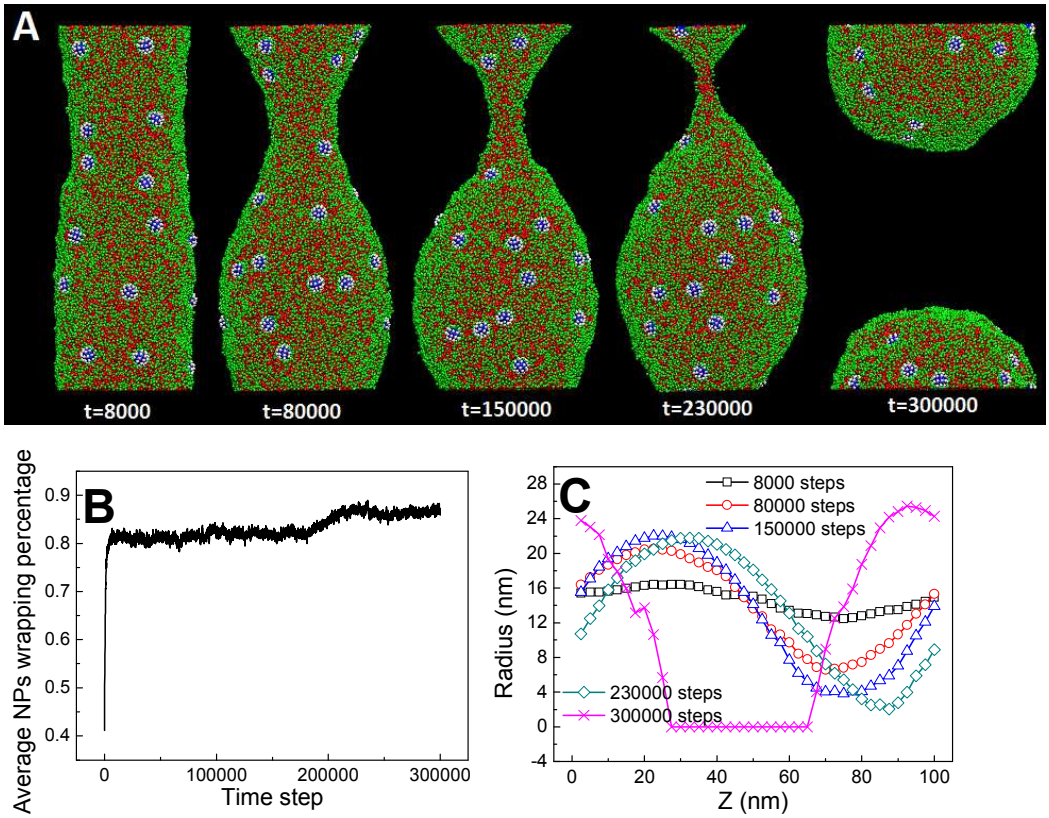

Fig. 4 The promotive effect of NPs with diameter and number of 2.5nm and 30 on the membrane tube pearling. A shows the time sequence of typical snapshots, B shows the time evolution of average wrapping extent of NPs, and C shows the corresponding distribution of membrane tube radius.

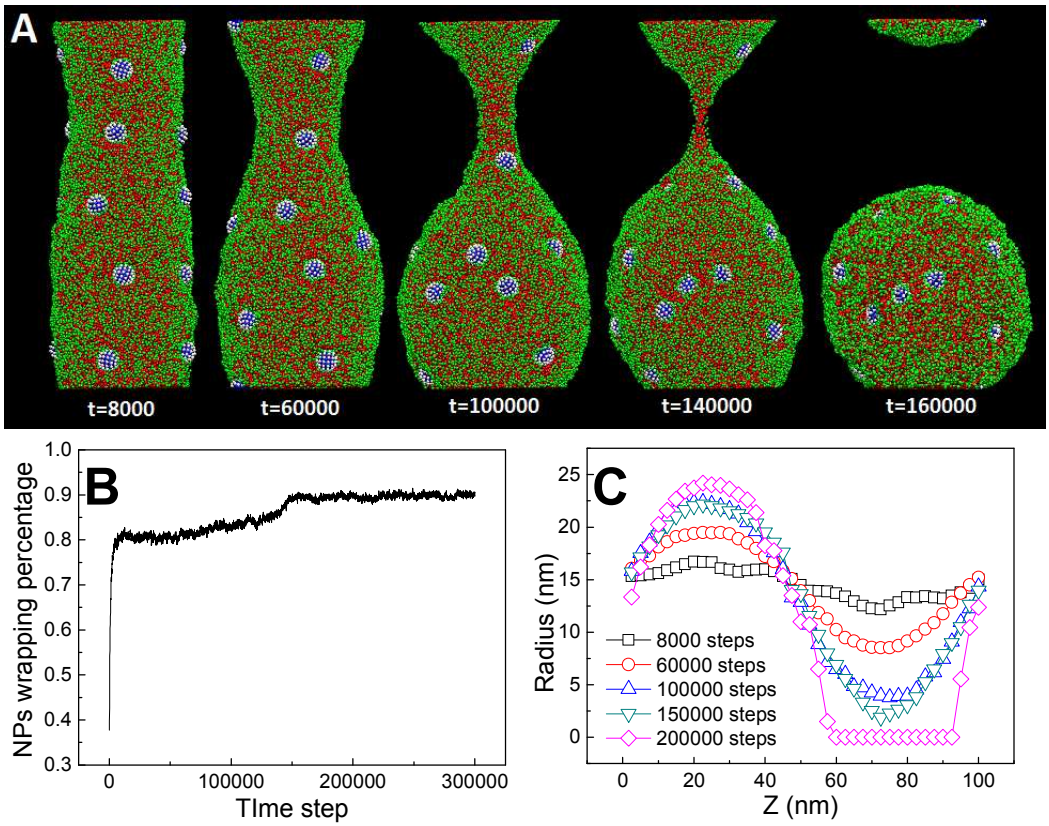

Fig. 5 The promotive effect of NPs with diameter and number of 3.8nm and 20 on the membrane tube pearling. A shows the time sequence of typical snapshots, B shows the time evolution of average wrapping extent of NPs, and C shows the corresponding distribution of membrane tube radius.

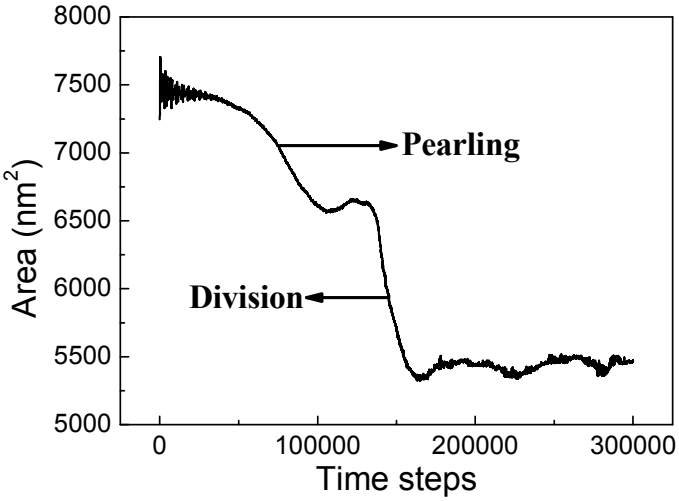

Fig. 6 Time evolution of membrane tube area during the pearling and division process. The water number inside the tube is fixed to 66000. The NP size and number are fixed to 3.8nm and 20, respectively.

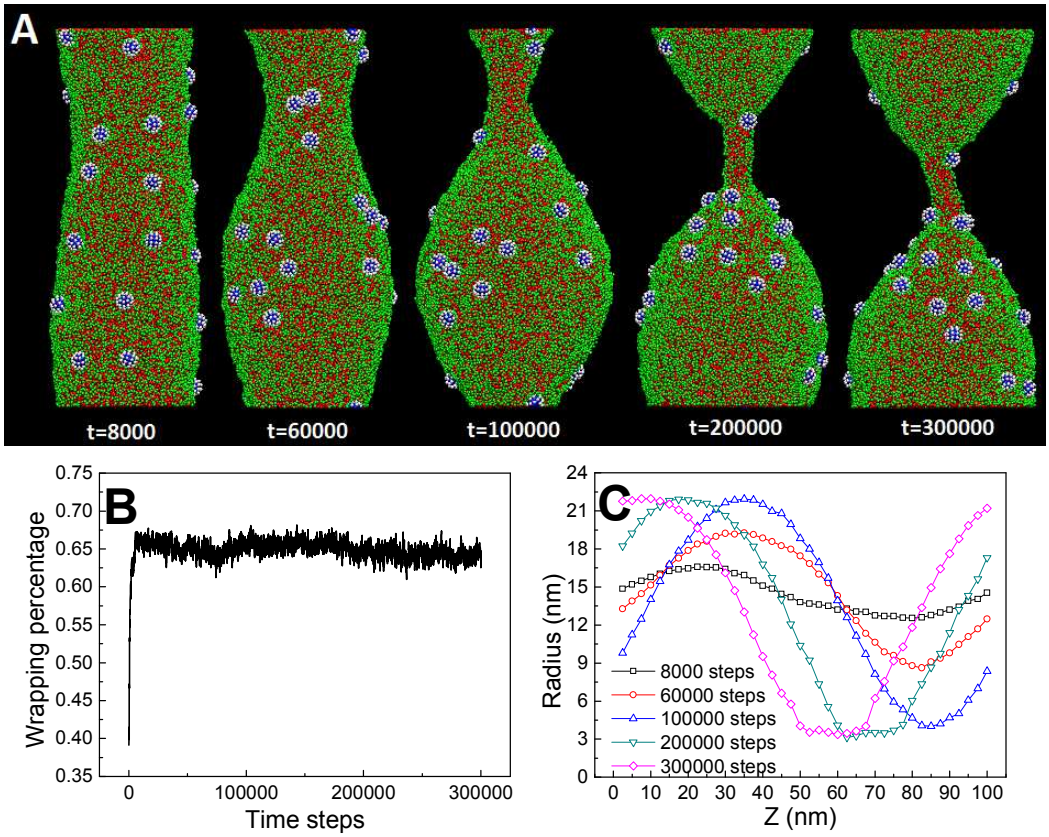

Fig. 7 The negligible effect of NPs with diameter and number of 2.5nm and 30 on the membrane tube pearling. The NP-membrane adhesion strength is decreased by fixing the interaction parameter a_{LH} to 10.0. A shows the time sequence of typical snapshots, B shows the time evolution of average wrapping extent of NPs, and C shows the corresponding distribution of membrane tube radius.

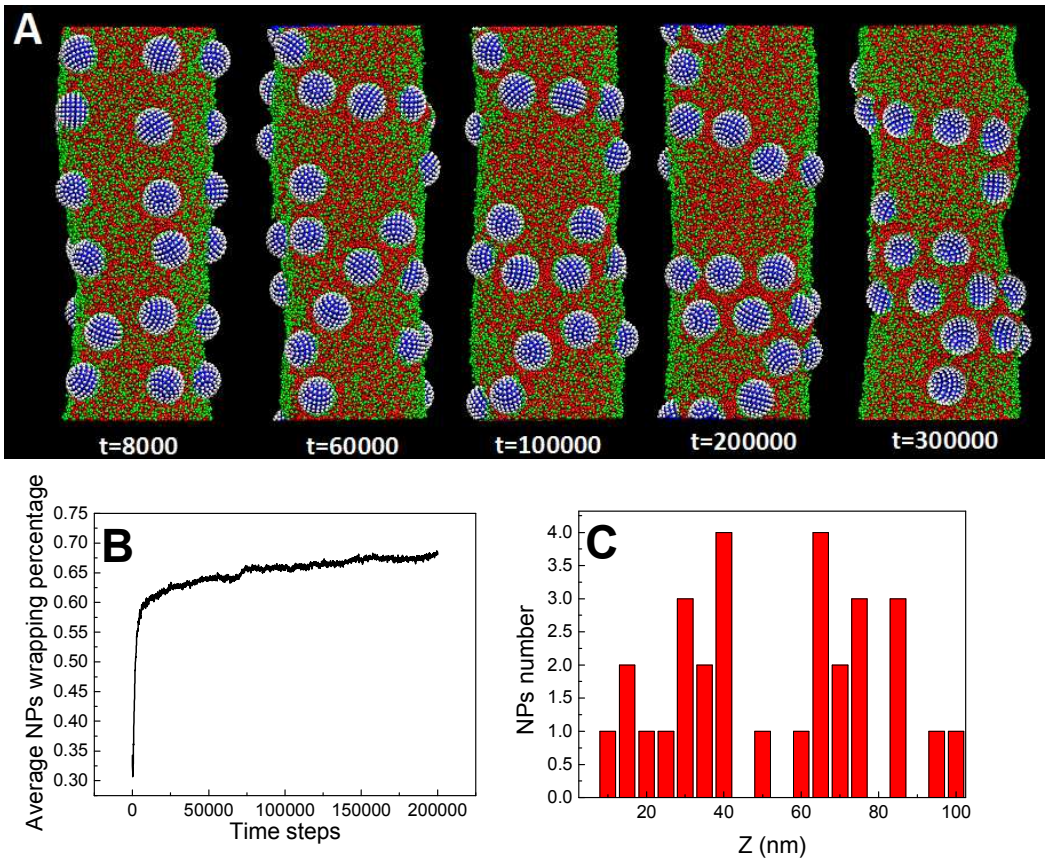

Fig. 8 The restraining effect of NPs with diameter and number of 7.5nm and 30 on the membrane tube pearling. A shows the time sequence of typical snapshots, B shows the time evolution of average wrapping extent of NPs, and C shows the final distribution of NPs along membrane tube direction.

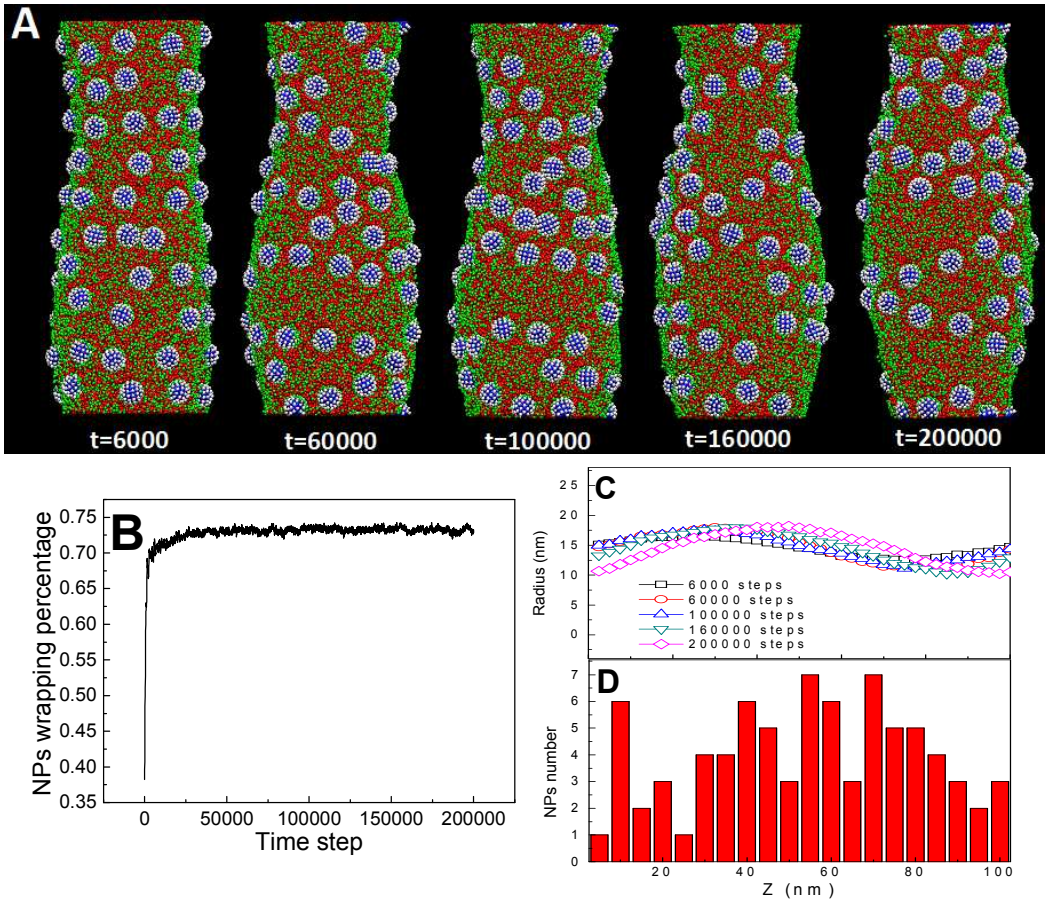

Fig. 9 The restraining effect of NPs with diameter and number of 3.8nm and 80 on the membrane tube pearling. A shows the time sequence of typical snapshots, B shows the time evolution of average wrapping extent of NPs, C shows the corresponding distribution of membrane tube radius, and D shows the final distribution of NPs along membrane tube direction.

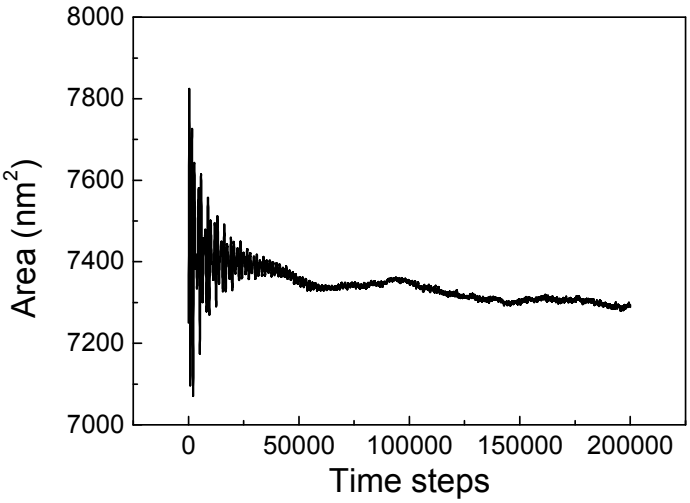

Fig. 10 Time evolution of tube area in the presence of NPs. The NP diameter and number are fixed to 3.8 and 80, respectively. The water number inside the tube is fixed to 66000.

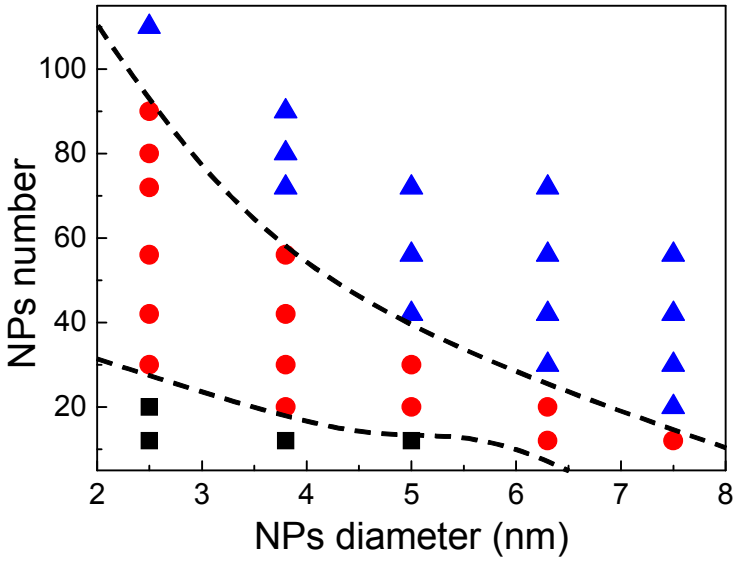

Fig. 11 Phase diagram of the effect of NPs adsorption on membrane tube pearling as functions of NP size and NP concentration. □ represents the negligible effect, ○ represents the promotive effect and △ represents the restraining effect. Note that the interaction parameter a_{LH} is fixed to 0.0.